Enhanced performance in dye-sensitized solar cell via laser generated noble metal nanoparticles treatment of photoelectrode

N. NASR, M. H. SAYYAD*
Faculty of Engineering Sciences, Ghulam Ishaq Khan Institute of Engineering Sciences and Technology, Topi, District Swabi, Khyber Pakhtunkhwa 23640, Pakistan

To improve the conversion efficiency of dye-sensitized solar cell, the cell was fabricated employing silver nanoparticles doped photoanode. The nanoparticles of silver were produced using the pulsed laser ablation technique. The I-V characteristics and impedance spectroscopic measurements were performed on the doped and undoped photoanode based devices under simulated AM 1.5 illumination (100 $mWcm^{-2}$) and dark, respectively. The nanoparticles doped photoanode based plasmonic DSSC exhibited about 46.3 % higher efficiency than the reference cell. This boosted performance of the plasmonic DSSC can be attributed to enhanced interfacial charge transfer, decrease of charge recombination, decrease of series resistance and plasmonic enhanced absorption of radiation by the dye. The impedance spectra also revealed higher photovoltaic performance of the plasmonic cell.

(Received June 8, 2018; accepted November 29, 2018)

Keywords: Dye-sensitized solar cells, Efficiency enhancement, High performance TiO_2 photoanode, Silver nanoparticles, Surface plasmon resonance (SRP) effect

1. Introduction

Dye-sensitized solar cells (DSSCs), originally demonstrated by O'Regan and Gratzel in 1991, have been extensively researched due to their ease of fabrication, clean source of renewable energy, different colors, potential for Building Integrated PhotoVoltaics (BIPV), availability of numerous alternative materials for lowering cost, improving stability and enhancing efficiency [1-8]. Extensive work is being done on the development and optimization of this next generation photovoltaic technology employing environmental-friendly materials [9, 10] with economical prices [5, 10], prolonged stability [11], and improved efficiency [12]. DSSC comprises a wide band gap semiconductor photoanode with a monolayer of a dye, a counter electrode and an electrolyte solution inserted inside the sandwiched electrodes. When solar radiation falls on the surface of a DSSC, the absorption of photons lead to the excitation of sensitizer molecules [13, 14]. Thereafter, the sensitizer molecules inject electrons into the conduction band of the TiO_2, and afterwards by diffusion these electrons go to the FTO. From there, via the external circuit, the electrons reach the counter electrode. The sensitizing dye is oxidized by transferring the electron to the TiO_2. This oxidized dye becomes neutralized by getting an electron from the iodide ion present in the electrolyte. Upon oxidizing, the iodide ion is converted to triiodide ion which further moves towards the counter electrode by the diffusion mechanism and hence taking an electron from the counter electrode, it becomes the iodide ion [15]. Thus, providing electrical energy to the external load.

Performance enhancement of DSSCs is an area of continued scientific research. One way of achieving this is to enhance its light harvesting and light trapping capabilities via surface modification of TiO_2 based nanomaterials with noble metal nanoparticles, like Ag, Al or Au nanoparticles [16-18]. These metals have robust capability of scattering effect as well as localized surface plasmon resonance (LSPR). This is so influential phenomenon which develops a strong electromagnetic field in the locality of these noble nanoparticles, consequentially, the photocurrent of DSSC boosts up as compared to the original current of DSSC [19]. The enhancement in the photocurrent by the localized electromagnetic field of noble metals results, in more efficient HOMO and LUMO transitions of the electrons in the dye molecules than the incident far field light [20]. Thus, the noble metal particles serve as light garnering probes for dyes [21, 22]. These noble metal nanoparticles used in DSSC require high purity and stability. Nanoparticles produced via different techniques have widely been adopted in DSSCs since its birth. The colloidal metal nanoparticles obtained via laser ablation are ligand-free and surface-clean [23]. Also, large scale production with controlled properties of NPs is attainable by this method [24].

In this work, nanoparticles of silver were produced using the pulsed laser ablation technique. Dye-sensitized solar cells were fabricated employing the undoped and silver nanoparticles doped titania photoanodes.

Photovoltaic and impedance spectroscopic measurements were performed under the radiance of 100 mW cm^{-2} (AM 1.5) and under the dark, respectively. This study may provide deep insight into the enhanced performance of the plasmonic DSSC and the processes involved, such as, the decrease of charge recombination, decrease of series resistance, increase of shunt resistance, decrease of ideality factor, etc.

2. Experimental details

2.1. Preparation of silver nanoparticle dispersion

Silver nanoparticle dispersion was synthesized using the pulsed laser ablation (PLA) technique. The silver pellet was placed in a beaker containing deionized water and was fired by the Quantel's nanosecond Q-switched pulsed Nd:YAG laser (Model Brilliant B) operated at its second harmonic wavelength of 532 nm and at frequency 10 Hz for about 30 minutes in free running mode, which resulted in a colloidal solution of the Ag nanoparticles.

2.2. Preparation of silver nanoparticle doped TiO_2 photoanode

The mesoporous titania electrode at about 80 ^oC was dipped in the nanoparticle dispersion of silver for about 16 hours, changing the color of the photoanode from crystal clear to yellowish after Ag nanoparticles were attached to TiO_2.

2.3. Fabrication of the reference and plasmonic DSSCs

The undoped and silver nanoparticles doped mesoporous titania electrodes at about 80 ^oC were soaked in the N719 dye solution in ethanol and were left for staining for about 16 hours. Subsequently, the sensitized photoanodes were taken out, washed carefully with ethanol and dried up with nitrogen gas. Afterwards, 60 μm thick Meltonix 1170-60 PF spot gasket was positioned on the top surface of anode over the titania area, the conductive side of Pt counter-electrode was placed over the gasket and immediately heated up to 100℃. After sealing, through the drilled hole, an iodide-based electrolyte of tri-iodide in acetonitrile (Solarnix, AN-50) was injected. The hole was then sealed with the Meltonix spot sealing and the glass spot cap. In addition to the silver nanoparticles, all the chemicals and substrates used for the assembly of DSSCs were acquired from Solaronix, Switzerland. The solvents were purchased from Sigma–Aldrich, United States. Active area of the cell was 0.36 cm^2.

2.4. Photovoltaic and impedance spectroscopy measurements

The photovoltaic and impedance spectroscopy parameters of the fabricated cells were measured using Keithley 4200-SCS equipped with a digital capacitance meter (model 4210-CVU) under dark and at AM 1.5 simulated illuminations (OAI TriSOL, AM1.5G Class AAA, USA). The power was set to 100 $mWcm^{-2}$ using Newport Oriel PV reference cell system (Model 91150V). Impedance spectra were studied applying a 30 mV AC signal from 1 kHz to 10 MHz.

3. Results and discussion

3.1. Photovoltaic performance

The characteristic photovoltaic parameters desired for the evaluation of the cells can be drawn out from the current density–voltage (J-V) characteristics. The J-V curves of the plasmonic and reference DSSCs fabricated using N719 dye as a sensitizer are compared in figure 1. In general, the efficiency (η) of a device is the output to the input power of the device. In case of a solar cell output is in the form of electric power and the input is the optical power incident on the cell. The cell efficiency can be calculated through the Eq. 1.

$$\eta = \frac{J_{sh} \times V_{oc} \times FF}{P_{in}} \tag{1}$$

where J_{sh}, V_{oc}, P_{in} and FF represent the short circuit current density, open circuit voltage, incident optical power and fill factor, respectively. The fill factor can be obtained using Eq. 2.

$$FF = \frac{J_{max} \times V_{max}}{J_{sc} \times V_{oc}} \tag{2}$$

where V_{max} and J_{max} represent the maximum voltage and the maximum current density at the peak output power point of the cell, respectively. The J-V curves greatly depend on the shunt (R_{sh}) and series (R_s) resistances [25]. The resistance due to recombination at contact interfaces, charge transfer in TiO_2 and sheet resistance of the electrodes are responsible for the series resistance (R_s) of the device. For improvement in device performance, the fill factor should be high enough. High R_s results in dropping the fill factor that in turn decreases the maximum power output of the device.

The electron dynamics at the semiconductor/dye/electrolyte interface is responsible for the device shunt resistance which offers an alternative route for the photo-generated current. The recombination at these interfaces are as the results of the crystal defects in the semiconductor material [26, 27]. The reduced shunt resistance means the high power loss in the device. The series and shunt resistances are obtainable from the J-V curve (Fig. 1) by means of the following relations [28].

$$R_s = \left.\frac{dV}{dJ}\right|V = 0 \tag{3}$$

$$R_{sh} = \left.\frac{dV}{dJ}\right|_{J=0} \quad (4)$$

Another key parameter which governs the DSSC mechanisms is the ideality factor n and its value under light can be obtained using Eq. 5 [29].

$$n = \left(\frac{k_B T}{q}\frac{d}{dV}\ln\frac{J}{J_o}\right)^{-1} \quad (5)$$

where J_o represents saturation current density, q is the electron charge, V is the applied voltage, and k_B is the Boltzmann constant. The recombination in the device is high if the value of n is high and vice versa.

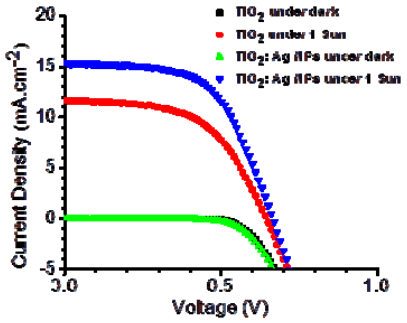

Fig. 1. J-V curves in the dark and under AM 1.5 illumination on TiO_2 and TiO_2:Ag NPs photoanodes based DSSCs.

Table 1. Parameters of undoped and doped photoanodes based DSSCs

Photoanode	J_{sc} ($mA.cm^{-2}$)	V_{oc} (mV)	FF (%)	η (%)	n	R_{sh} (Ω)	R_s (Ω)
Undoped	11.7	640	55.6	4.1	1.7	1466	16
Doped	15.4	670	57.8	6.0	1.2	2133	11

The important parameters extracted from the J-V characteristics of the TiO_2 and TiO_2:Ag NPs photoanodes based DSSCs are listed in Table 1.

It is noticeable that the η of plasmonic DSSC (6.0 %) is much higher than the reference cell (4.1%). The values of J_{sc} (15.4 mA/cm^2), V_{oc} (670 mV) and FF (57.8 %) of doped photoanode based DSSC have all increased as compared to the reference cell based on undoped photoanode. The overall η, J_{sc}, V_{oc}, and FF of the plasmonic cells were observed greater than the reference cell by 46.3 %, 31.6 %, 4.7 %, and 3.9 %, respectively. This enhanced performance of the plasmonic DSSC over the reference cell may be due to the light trapping effect, reduction in the electrons recombination and the boosted absorption of radiation by the dye [17, 18, 30]. The enhancement in J_{sc} may be credited to the better interconnectivity of TiO_2 particles and the Ag NPs in the porous TiO_2 film. The treatment of the TiO_2 via Ag NPs provides more efficient electron transfer in DSSCs. Surface plasmon resonance (SRP) effect given by the Ag NPs boosts the neighboring electromagnetic fields, because of this enhancement the capability of photon captivation by the dye molecules increases, which in turn increases the exciton generation and dissociation and hence increases the device photocurrent.

The relatively higher performance of plasmonic DSSC may be attributed to the lowered series resistance and higher shunt resistance. The increase of R_{sh} in the case of plasmonic DSSC specifies the comparatively fewer shorts in the Ag doped DSSC. The boosted comportment of the plasmonic cell may also be ascribed due to the decrease in its ideality factor. The percentage increase of η and J_{sc}, observed in this work are much higher than reported in a recent study on efficiency improvement in dye sensitized solar cells by the plasmonic effect of green synthesized silver nanoparticles [23]. This may be attributed due to the clean nature of laser generated nanoparticles dispersion employed in this work.

3.2. Impedance spectroscopy

To boost the efficiency, develop stable and lower cost DSSC technology, the researchers are working to improve the various components of this technology, such as, semiconductor, sensitizer, electrolyte, counter electrode, photoanode and interfaces involved. These different components and interfaces can be modeled by equivalent electrical circuits comprising electrical components.

In this work, the DSSCs are replaced by their equivalent series and parallel measurement models [31], and impedance spectroscopy is performed to probe into the electrical properties of the DSSCs fabricated using TiO_2 and TiO_2:Ag NPs photoanodes. The wealth of data obtained through these experimental studies may be useful for (i) evaluating the performance of solar cells, (ii) testing and developing the solar cell models, (iii) examining the role of different components and interfaces affecting the DSSC performance, (iv) knowing causes of cell degradation, (v) knowing the processes required to be optimized during the preparation of cell components for its better performance.

Electrochemical impedance spectroscopy (EIS) has been performed in order to investigate the kinetic processes within the DSSC and the impedance data for a DSSC is reported to consist of three semicircles in the Nyquist plot [32, 33]. These three semicircles denote the responses in high-frequency, intermediate-frequency and low-frequency regions when the solar cell is biased at its V_{OC} [33]. The high frequency region is due to the charge transfer between the electrolyte and counter electrode interface while intermediate-frequency is attributed due to the electron transport in the dye-sensitized semiconductor

layer and the recombination process at the dye-sensitized layer and the electrolyte interface. The low-frequency region represents the diffusion process in the electrolyte.

3.2.1. Parallel capacitance – voltage (C_P-V) characteristics

Results of frequency dependent capacitance – voltage studies on the TiO_2 and TiO_2: Ag NPs photoanodes based DSSCs are shown in Fig. 2. For the voltage sweep from -1.0 to +1.0 volts, at lower frequencies, the devices exhibit an increasing behavior in the capacitance. This increase in capacitance reaches up to certain maximum value and after then a decline in the capacitance value may be observed.

Some extra peaks, not observed in the Nyquist plots, are exhibited at low frequencies and are attributed due to series resistance and interface states[34].

As shown in the graph (Fig. 2) at high frequencies, declination towards zero or even negative capacitance is observed which may be due to the fact that up to certain frequencies the probe signal is followed by the trap states but at large frequencies the probe signal is quicker and trap states are unable to follow them as a result probe signal respond is zero which is the mean value of the oscillation. [35]. Similar behavior of capacitance at high frequencies has also been reported in other DSSCs studies [34, 36]. The physical phenomena behind the positive to negative shift in capacitance is the electrons injection in the semiconducting surface from the FTO in the DSSC [36].

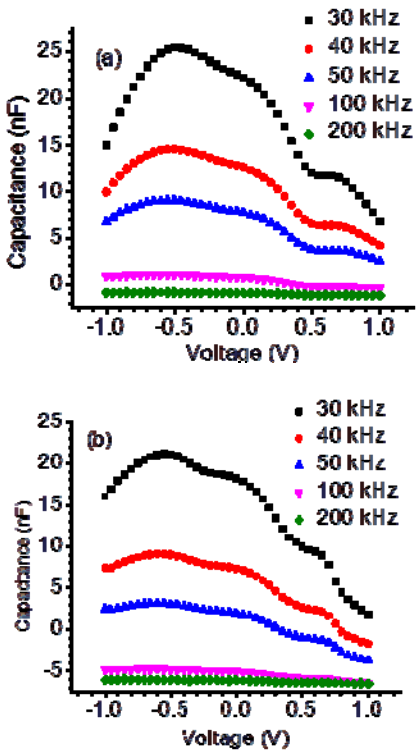

Fig. 2. C_p-V curves recorded at different frequencies in the dark on (a) TiO_2 and (b) TiO_2:Ag NPs photoanodes based DSSCs.

3.2.2. Series resistance – voltage (R_s-V) and series capacitance – voltage (C_s-V) characteristics

Similar to the EIS studies [33], three characteristic regions are observed in the frequency dependent series resistance versus voltage and series capacitance versus voltage characteristics of DSSCs. The lower frequencies reflect the diffusion aptitude of the redox species inside the electrolyte, the mid frequencies domain arises from the electron transfer processes between the semiconducting oxide and electrolyte interface while the higher side represents the charge transport behavior at the platinum electrode [37].

The frequency dependent series resistance versus voltage and series capacitance versus voltage characteristics of TiO_2 and TiO_2:Ag NPs photoanodes based DSSCs measured at mid and high frequencies are exhibited in figures 3 and 4, respectively. Both the resistance and capacitance characteristics persist non-responded around the unbiased low voltage regime. When the applied voltage is increased, the resistance and capacitance are observed voltage and frequency dependent. This voltage and frequency dependence of the impedance spectra of DSSCs may be attributed due to several causes, already described in our earlier study [7].

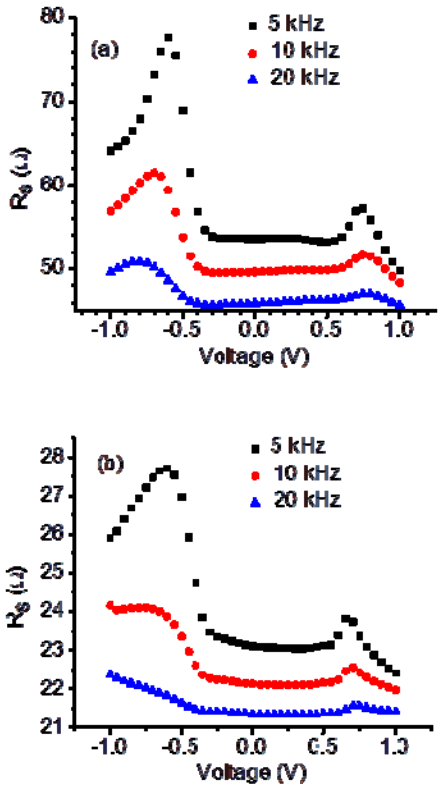

Fig. 3. R_s-V plots taken at various frequencies in the darker conditions (a) TiO_2 and (b) TiO_2:Ag NPs photoanodes based DSSCs.

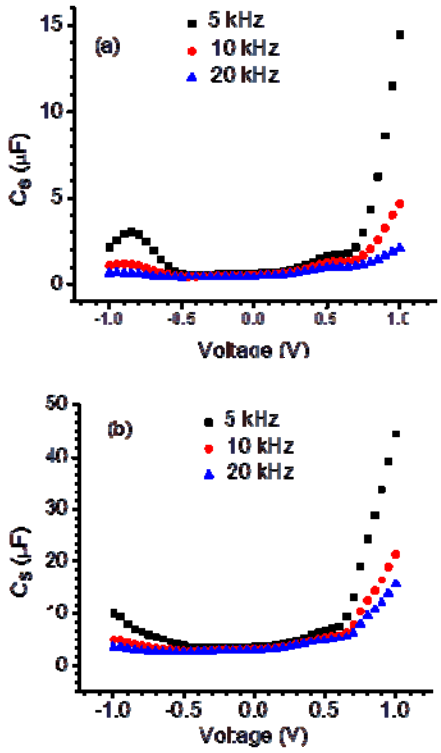

Fig. 4. C_s-V plots taken at various frequencies in the darker conditions (a) TiO_2 and (b) TiO_2:Ag NPs photoanodes based DSSCs.

At lower frequencies and higher applied bias voltages, the impedance spectra compared in Figs. 3 and 4. These spectra are dominated by the recombination resistance and chemical capacitance [38, 39] and are in agreement with the enhanced photovoltaic performance exhibited by the plasmonic device.

4. Conclusions

On the basis of photovoltaic measurements and impedance spectroscopy, a relative evaluation of the TiO_2 and TiO_2:Ag NPs photoanodes based DSSCs has been performed. The J-V characteristics have revealed better photovoltaic behavior of the plasmonic DSSC. The C_p-V, R_s-V, C_s-V along with impedance measurements on the TiO_2 and TiO_2:Ag NPs photoanodes based cells were examined. An understanding into the better photovoltaic performance exhibited by the plasmonic DSSC is presented. This may be attributed due to increase in shunt resistance, the boosted photonic absorption of the dye due to plasmonic behavior, decrease in the series resistance, and decrease in the ideality factor. The measured performance of the fabricated DSSCs is established from the comparative study of the recombination resistance and chemical capacitance.

Acknowledgements

We greatly appreciate the financial support provided by the HEC Pakistan and US National Academy of Sciences, under the PAK-US Science and Technology Cooperation Program, Phase-V, project number 5-530/PAK-US/HEC/2013/193.

References

[1] B. O'regan, M. Grätzel, Nature **353**, 737 (1991).
[2] D. Joly, L. Pellejà, S. Narbey, F. Oswald, J. Chiron, J. N. Clifford et al., Scientific Reports **4**, 2014.
[3] D. Joly, L. Pelleja, S. Narbey, F. Oswald, T. Meyer, Y. Kervella et al., Energy & Environmental Science **8**, 2010 (2015).
[4] S. Sigdel, H. Elbohy, J. Gong, N. Adhikari, K. Sumathy, H. Qiao et al., IEEE Transactions on Electron Devices **62**, 2027 (2015).
[5] H. Elbohy, A. Aboagye, S. Sigdel, Q. Wang, M. H. Sayyad, L. Zhang et al., Journal of Materials Chemistry A **3**, 17721 (2015).
[6] S. A. A. Shah, M. H. Sayyad, F. Wahab, K. A. Khan, M. A. Munawar, H. Elbohy et al., Journal of Materials Science: Materials in Electronics **27**, 4501 (2016).
[7] S. A. A. Shah, M. H. Sayyad, N. Nasr, R. A. Toor, S. Sajjad, H. Elbohy et al., Journal of Materials Science: Materials in Electronics **28**, 6552 (2017).
[8] P. Gu, D. Yang, X. Zhu, H. Sun, P. Wangyang, J. Li et al., AIP Advances **7**, 105219 (2017).
[9] C.-P. Lee, C.-T. Li, K.-C. Ho, Materials Today **20**, 267 (2017).
[10] H. Hug, M. Bader, P. Mair, T. Glatzel, Applied Energy **115**, 216 (2014).
[11] G. G. Sonai, A. Tiihonen, K. Miettunen, P. D. Lund, A. F. Nogueira, The Journal of Physical Chemistry C **121**, 17577 (2017).
[12] Ö. Ateş Sönmezoğlu, S. Akın, B. Terzi, S. Mutlu, S. Sönmezoğlu, Advanced Functional Materials **26**, 8776 (2016).
[13] J. Nissfolk, K. Fredin, A. Hagfeldt, G. Boschloo, The Journal of Physical Chemistry B **110**, 17715 (2006).
[14] M. Grätzel, Journal of Photochemistry and Photobiology A: Chemistry **164**, 3 (2004).
[15] B. E. Hardin, H. J. Snaith, M. D. McGehee, Nature Photonics **6**, 162 (2012).
[16] Y. Zhang, R. Huang, X. Zhu, L. Wang, C. Wu, Chinese Science Bulletin **57**, 238 (2012).
[17] A. Zhang, Z. Guo, Y. Tao, W. Wang, X. Mao, G. Fan et al., Nanoscale Research Letters **10**, 214 (2015).
[18] G. Dai, R. Wu, A. Zhang, X. Bao, H. Zhou, F. Shen et al., J. Optoelectron. Adv. M. **18**(7-8), 618 (2016).
[19] G. Spyropoulos, M. Stylianakis, E. Stratakis, E. Kymakis, Photonics and Nanostructures-Fundamentals and Applications **9**, 184 (2011).
[20] Y. Xu, H. Zhang, X. Li, W. Wang, J. Li, Journal of . Alloys and Compounds **695**, 1104 (2017).
[21] P. Joshi, L. Zhang, D. Davoux, Z. Zhu, D. Galipeau,

H. Fong et al., Energy & Environmental Science **3**, 1507 (2010).
[22] K. U. Isah, B. J. Jolayemi, U. Ahmadu, M. I. Kimpa, N. Alu, Materials for Renewable and Sustainable Energy **5**, 10 (2016).
[23] J. Zhang, J. Claverie, M. Chaker, D. Ma, ChemPhysChem **18**(9), 986 (2017).
[24] P. Kazakevich, A. Simakin, V. Voronov, G. A. Shafeev, Applied Surface Science **252**, 4373 (2006).
[25] S. S. Mali, C. Betty, P. Bhosale, P. Patil, Electrochimica Acta **59**, 113 (2012).
[26] N. Koide, A. Islam, Y. Chiba, L. Han, Journal of Photochemistry and Photobiology A: Chemistry **182**, 296 (2006).
[27] T. Hanmin, Z. Xiaobo, Y. Shikui, W. Xiangyan, T. Zhipeng, L. Bin et al., Solar Energy **83**, 715 (2009).
[28] C. Jiang, X. Sun, K. Tan, G. Lo, A. Kyaw, D. Kwong, Applied Physics Letters **92**, 143101 (2008).
[29] U. Würfel, D. Neher, A. Spies, S. Albrecht, Nature Communications **6**, 6951 (2015).
[30] S. Buda, S. Shafie, S. A. Rashid, H. Jaafar, N. Sharif, Results in Physics **7**, 2311 (2017).
[31] J. Carr, S. Chaudhary, Applied Physics Letters **100**, 213902 (2012).
[32] Q. Wang, J.-E. Moser, M. Grätzel, The Journal of Physical Chemistry B **109**, 14945 (2005).
[33] H. Jun, M. Careem, A. Arof, Materials Today: Proceedings **3**, S73 (2016).
[34] I. Yahia, S. AlFaify, A. A. Al-ghamdi, H. S. Hafez, S. EL-Bashir, A. Al-Bassam et al., Applied Physics A **122**, 1 (2016).
[35] M. Samadpour, P. P. Boix, S. Giménez, A. Iraji Zad, N. Taghavinia, I. Mora-Seró et al., The Journal of Physical Chemistry C **115**, 14400 (2011).
[36] M. Atif, W. Farooq, A. Fatehmulla, M. Aslam, S. M. Ali, Materials **8**, 355 (2015).
[37] J. Idigoras, R. Tena-Zaera, J. A. Anta, Physical Chemistry Chemical Physics **16**, 21513 (2014).
[38] D. Joly, L. Pellejà, S. Narbey, F. Oswald, J. Chiron, J. N. Clifford et al., Scientific Reports **4**, 4033 (2014).
[39] J. Bisquert, Physical Chemistry Chemical Physics **5**, 5360 (2003).

*Corresponding author: hsayyad62@gmail.com;
sayyad@giki.edu.pk